College of Arts and Sciences

Drexel E-Repository and Archive (iDEA)
http://idea.library.drexel.edu/

Drexel University Libraries
www.library.drexel.edu

The following item is made available as a courtesy to scholars by the author(s) and Drexel University Library and may contain materials and content, including computer code and tags, artwork, text, graphics, images, and illustrations (Material) which may be protected by copyright law. Unless otherwise noted, the Material is made available for non profit and educational purposes, such as research, teaching and private study. For these limited purposes, you may reproduce (print, download or make copies) the Material without prior permission. All copies must include any copyright notice originally included with the Material. **You must seek permission from the authors or copyright owners for all uses that are not allowed by fair use and other provisions of the U.S. Copyright Law.** The responsibility for making an independent legal assessment and securing any necessary permission rests with persons desiring to reproduce or use the Material.

Please direct questions to archives@drexel.edu

arXiv:0709.1479v1 [astro-ph] 11 Sep 2007

Weak lensing ellipticities in a strong lensing regime

Richard Massey[1] & David M. Goldberg[2]

ABSTRACT

It is now routine to measure the weak gravitational lensing shear signal from the mean ellipticity of distant galaxies. However, conversion between ellipticity and shear assumes local linearity of the lensing potential (*i.e.* that the spatial derivatives of the shear are small), and this condition is not satisfied in some of the most interesting regions of the sky. We extend a derivation of lensing equations to include higher order terms, and assess the level of biases introduced by assuming that first-order weak lensing theory holds in a relatively strong shear regime. We find that, even in a worst-case scenario, a fully linear analysis is accurate to within 1% outside ~ 1.07 times the Einstein radius of a lens. The effect should therefore have little impact on measurements of overall cluster masses for the foreseeable future. However, at the level of accuracy demanded by upcoming lensing surveys, such biases ought to be considered in measurements of the inner slope of cluster mass distributions and the small-scale end of the mass power spectrum. Both of these are central in determining the relationship between baryonic and dark matter.

Subject headings: gravitational lensing

1. Introduction

Gravitational lensing is the deflection of light rays from a background light source by an intervening gravitational field (Mellier 1999; Refregier 2003). It is one of the most promising probes of the distribution of invisible dark matter in the Universe, and hence the effects of dark energy. Gravitatational lensing comes in two flavors. "Strong lensing" is rare, but where the deflection is sufficient, image distortion can be visible in individual (often multiply imaged) background galaxies. Along most lines of sight through the universe, even those passing through the outskirts of galaxy clusters, only "weak lensing" is produced. The weaker signal has to be collected statistically and, to first order in a Taylor series, it is obtained from the mean ellipticity of an otherwise uncorrelated set of galaxies (Bartelmann & Schneider 2000).

Since only a few, choice lines of sight present a strong lensing signal, weak lensing measurements alone are frequently used to map the distribution of mass (Clowe et al. 2006; Massey et al. 2007; Gavazzi & Soucail 2007) or characterize its large-scale statistical properties (Massey et al. 2007; Benjamin et al. 2007; Kitching et al. 2007). However, it is often the most massive structures that are of particular interest in the maps (*e.g.* Wittman 2005; Schirmer et al. 2007; Miyazaki et al. 2007), and that dominate the contribution to the power spectrum on small scales (*e.g.* Smith et al. 2003). Near such regions, the assumptions implicit in a weak lensing analysis no longer necessarily hold. In this paper, we expand the Taylor series of the weak lensing equation to include the next-highest terms, and investigate the level of bias in shear measurements that rely upon simple measurements of ellipticity. These biases operate in addition to those discussed by the Shear TEsting Programme (STEP: Heymans et al. 2006; Massey et al. 2007), which has currently tested only the explicitly weak lensing regime.

This paper is structured as follows: in §2, we derive the lensing equations, in §3, we check our results using raytraced simulations, and we discuss their implications in §4.

[1]California Institute of Technology, 1200 East California Boulevard, Pasadena, CA 91125, U.S.A.

[2]Department of Physics, Drexel University, 3141 Chestnut Street, Philadelphia, PA 19104, U.S.A.

2. Lensing Transformations

2.1. The Usual First-Order Treatment

A general gravitational lens deflects a light from a position x' in a background (source) image to a position x in the observed (lens) plane, such that

$$\vec{x'} = \vec{x} - \vec{\alpha}(\vec{x}) \ , \tag{1}$$

with a deflection angle predicted by General Relativity in the weak field limit of

$$\vec{\alpha}(\vec{x}) = \vec{\nabla}\Psi(\vec{x}) \ , \tag{2}$$

and where $\Psi(\vec{x})$ is the Newtonian potential of the lens, $\Phi(\vec{x}, z)$, projected onto the plane of the sky.

Crucially, the gravitational field and the deflection angle vary across the sky. Assuming the (local linearity) condition that the change is linear on scales the size of a galaxy, it can be described to first order by a coordinate transformation

$$x'_i = x_i - \left[\frac{\partial\Psi}{\partial x_i}\right] - \frac{\partial}{\partial x_j}\left[\frac{\partial\Psi}{\partial x_i}\right]\Delta x_j + ... \ . \tag{3}$$

The first derivative term on the right represents an unmeasurable centroid shift. Placing the origin of the coordinate system at the galaxy's observed center of light, we are left with

$$x'_i = \mathcal{A}_{ij}x_j + ... \ , \tag{4}$$

where the Jacobian of the transformation is

$$\mathcal{A}_{ij} = \delta_{ij} - \frac{\partial^2\Psi}{\partial x_i \partial x_j} \tag{5}$$

$$\mathcal{A} \equiv \begin{pmatrix} 1-\kappa-\gamma_1 & -\gamma_2 \\ -\gamma_2 & 1-\kappa+\gamma_1 \end{pmatrix} \ . \tag{6}$$

We have introduced the usual notation of convergence $\kappa = \vec{\nabla}^2\Psi/2$, which is thus proportional to the distribution of mass projected along a line of sight, and two components of shear γ_i.

It is always possible to adopt an arbitrary choice of rotation for the coordinate system such that $\gamma_2 = 0$ and $\mathcal{A}$ is diagonal. Hence the inverse mapping

$$x_i = (\mathcal{A})^{-1}_{ij}x'_j + ... \tag{7}$$

involves a simple matrix

$$\mathcal{A}^{-1} = \begin{pmatrix} \frac{1}{1-\kappa-\gamma_1} & 0 \\ 0 & \frac{1}{1-\kappa+\gamma_1} \end{pmatrix} \ . \tag{8}$$

We use parity symmetry to assume that the potential increases to the right (hence $\gamma_1 < 0$). We also work only in the "positive parity" lensing regime (outside the critical curve), where $\det\mathcal{A} > 0$, though this analysis is equally valid inside the critical curve.

The shape of a galaxy image $I(x')$ can be quantified via its intrinsic ellipticity

$$\left\{\chi_1^{\rm int}, \chi_2^{\rm int}\right\} \equiv \left\{\frac{Q_{11}^{\rm int} - Q_{22}^{\rm int}}{Q_{11}^{\rm int} + Q_{22}^{\rm int}}, \frac{2Q_{12}^{\rm int}}{Q_{11}^{\rm int} + Q_{22}^{\rm int}}\right\} \ , \tag{9}$$

where its quadrupole moments are

$$Q_{ij}^{\rm int} \equiv \frac{\int I(\vec{x'}) \ x'_i \ x'_j \ {\rm d}^2\vec{x'}}{\int I(\vec{x'}) \ {\rm d}^2\vec{x'}} \ . \tag{10}$$

Under the (locally linear) lensing transformation (7), the galaxy's observed ellipticity becomes

$$\chi_i^{\rm obs} = \chi_i^{\rm int} + 2\gamma_i - \chi_i^{\rm int}(\chi_j^{\rm int}\gamma_j) \ , \tag{11}$$

to first order in γ (*c.f.* Seitz & Schneider 1995). Averaging over a population of galaxies with uncorrelated intrinsic shapes $\langle\chi^{\rm int}\rangle = 0$, an estimator $\tilde{\gamma}$ can then be formed to recover the gravitational shear signal

$$\langle\tilde{\gamma_i}\rangle \equiv \frac{\left\langle\chi_i^{\rm obs}\right\rangle}{2 - \left\langle(\chi_i^{\rm int})^2\right\rangle} = \langle\gamma_i\rangle \ . \tag{12}$$

The variance in the denominator can be closely approximated by the observed value. The denominator is of order 1.6 (*e.g.* Massey et al. 2007).

For practical purposes, a weight function $W(\vec{x})$ with finite support is also usually applied to the integrals in equation (10). This complicates the normalization of the shear estimator: the shear polarizability tensor P^γ in Kaiser, Squires & Broadhurst (1995), which replaces the denominator of equation (12), depends upon derivatives of $W(\vec{x})$. However, P^γ is typically fitted from a large ensemble of galaxy shapes to reduce noise, and almost all of those galaxies will be along a line of sight unaffected by higher order lensing terms. We therefore ignore the effect[1].

[1] As pointed out during the derivation of "reduced shear" by Bartelmann & Schneider (2000), a galaxy's flux density $I(\vec{x'})$ could equally well be replaced in equation (10) and throughout by a monotonic function of intensity $f(I(\vec{x'}))$, without a change in the formalism. This approximates a useful weighting scheme.

We also ignore the blurring effect of a point-spread function, which needs to be corrected separately.

2.2. Higher order terms

Continuing the Taylor series in equation (3), we can write (see *e.g.* Goldberg & Natarajan 2002)

$$x'_i = \mathcal{A}_{ij}x_j - \frac{1}{2}\frac{\partial^3\Psi}{\partial x_i\partial x_j\partial x_k}x_jx_k - \frac{1}{6}\frac{\partial^4\Psi}{\partial x_i\partial x_j\partial x_k\partial x_l}x_jx_kx_l + ... \quad (13)$$

Repeatedly substituting the simple form

$$x_i = (\mathcal{A})^{-1}_{ij}\left(x'_j + \frac{1}{2}\Psi_{,jkl}\,x_kx_l + \frac{1}{6}\Psi_{,jklm}\,x_kx_lx_m\right) \quad (14)$$

into itself then yields the inverse mapping

$$\begin{aligned} x_i &= (\mathcal{A})^{-1}_{ij}x'_j \quad (15)\\ &+ {}^1\!/_2(\mathcal{A})^{-1}_{ij}(\mathcal{A})^{-1}_{kp}(\mathcal{A})^{-1}_{lq}\Psi_{,jkl}\,x'_px'_q\\ &+ {}^1\!/_6(\mathcal{A})^{-1}_{ij}(\mathcal{A})^{-1}_{kp}(\mathcal{A})^{-1}_{lq}(\mathcal{A})^{-1}_{mr}\Psi_{,jklm}\,x'_px'_qx'_r\\ &+ {}^1\!/_2(\mathcal{A})^{-1}_{ij}(\mathcal{A})^{-1}_{kp}(\mathcal{A})^{-1}_{lm}(\mathcal{A})^{-1}_{nq}(\mathcal{A})^{-1}_{sr}\\ &\qquad \Psi_{,jkl}\,\Psi_{,mns}\,x'_px'_qx'_r\\ &+ ... \end{aligned}$$

The various terms are listed in order of decreasing importance. Third derivatives of Ψ are related to the *flexion* signal (Goldberg & Bacon 2005; Bacon et al. 2006). This is small for realistic potentials; higher derivatives of Ψ will be smaller still. Note that this relation still holds locally even if there are multiple images, but that there will be different values of $\mathcal{A}$ at each image.

To complicate matters, this mapping now shifts the galaxy's center of light. If the background image were correctly centroided (*i.e.* $\langle x'\rangle = 0$), the observed centroid would be

$$\langle x_i\rangle \approx \frac{1}{2}(\mathcal{A})^{-1}_{ij}(\mathcal{A})^{-1}_{km}(\mathcal{A})^{-1}_{ln}\Psi_{,jkl}\,Q^{\rm int}_{mn}\ , \quad (16)$$

plus smaller contributions coming from the galaxy's intrinsic octopole moment. In a coordinate system centered on the observed image, the mapping is therefore

$$\begin{aligned} x_i &= (\mathcal{A})^{-1}_{ij}x'_j \quad (17)\\ &+ {}^1\!/_2(\mathcal{A})^{-1}_{ij}(\mathcal{A})^{-1}_{kp}(\mathcal{A})^{-1}_{lq}\Psi_{,jkl}\left(x'_px'_q - Q^{\rm int}_{pq}\right)\\ &+ {}^1\!/_6(\mathcal{A})^{-1}_{ij}(\mathcal{A})^{-1}_{kp}(\mathcal{A})^{-1}_{lq}(\mathcal{A})^{-1}_{mr}\Psi_{,jklm}\,x'_px'_qx'_r\\ &+ {}^1\!/_2(\mathcal{A})^{-1}_{ij}(\mathcal{A})^{-1}_{kp}(\mathcal{A})^{-1}_{lm}(\mathcal{A})^{-1}_{nq}(\mathcal{A})^{-1}_{sr}\\ &\qquad \Psi_{,jkl}\,\Psi_{,mns}\,x'_px'_qx'_r\\ &+ ... \ . \end{aligned}$$

In practice, a galaxy's intrinsic quadrupole moments cannot be observed. We compute them as a function of the galaxy's observed shape using equation (13). However, this produces an unwieldly general expression, because the quadrupole moments couple to several non-negligible coefficients during the transformation.

Equation (18) assumes a fully general potential which has been rotated to a convenient frame. To make the equations more tractable, we fix various properties of the lens and the source galaxy. We first set to zero all derivatives of Ψ that are "odd" at 90° ($\Psi_{,112}$, $\Psi_{,222}$, $\Psi_{,1112}$ and $\Psi_{,1222}$). For a circular (or nearly circular) potential that has been rotated so that $\Psi_{,12} = 0$, this assumption will be (nearly) accurate. It is also explicitly true at the major and minor axes of an elliptical potential.

Since we are in a fairly strong lensing regime, it is not unreasonable to assume that $\gamma \gg \chi^{\rm int}$, so the galaxy can be considered intrinsically circular. It still has a size $R^2 \equiv 2Q^{\rm int}_{11} = 2Q^{\rm int}_{22}$ and concentration index

$$c \equiv \frac{\int I(\vec{x})\ |\vec{x}|^4\ {\rm d}^2\vec{x}}{R^2\int I(\vec{x})\ {\rm d}^2\vec{x}}\ , \quad (18)$$

which would be 2 for a Gaussian, 10/3 for an exponential, and higher still for a de Vaucouleurs profile. The observed ellipticity becomes

$$\begin{aligned} \chi_1^{\rm obs} = \chi_1^{\rm lin} - \frac{a^2d^2}{4(a^2+d^2)^2}\frac{R^2}{}\Big[\big\{a^2\Psi_{,111} + d^2\Psi_{,122}\big\}^2 \quad (19)\\ -c\big\{15a^4\Psi^2_{,111} - (12a^2d^2 + 4ad^3 - 3d^4)\Psi^2_{,122}\\ -2a^2d(2a-3d)\Psi_{,111}\,\Psi_{,122}\\ +4a^3\Psi_{,1111} - 4ad(a-d)\Psi_{,1122} - 4d^3\Psi_{,2222}\big\}\Big]\ . \end{aligned}$$

where $a \equiv (\mathcal{A}^{-1})_{11} = (1-\Psi_{,11})^{-1}$ and $d \equiv (\mathcal{A}^{-1})_{22} = (1-\Psi_{,22})^{-1}$ are both unitless. It can be seen that the deviation from an ellipticity assuming local linearity, $\chi^{\rm lin}$, will tend as R^2/θ_E^2.

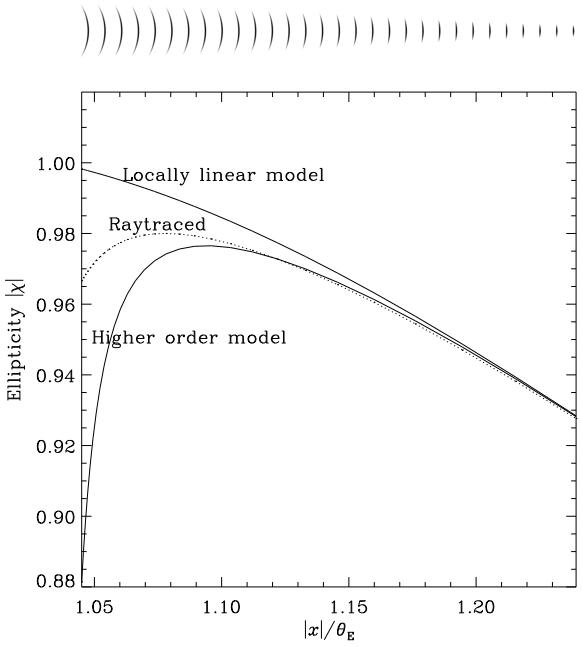

Fig. 1.— *Upper images*: The observed shape of an intrinsically circular galaxy with a Gaussian radial profile and size $\sigma = 0.01\theta_E$, at various positions behind a singular isothermal sphere lens. The images are presented with a logarithmic color stretch. *Main panel*: The solid lines show the object's ellipticity predicted by the usual linear model and our higher order model. The dotted line shows measured values from a fully raytraced simulation.

3. Verification through raytracing

We have developed a simple raytracing routine to deflect rays via equation (2), deforming the intrinsic shapes of source galaxies into arcs. The upper panel of figure 1 demonstrates the effect of a singular isothermal sphere lens with Einstein radius θ_E on an intrinsically circular Gaussian source with $\sigma = 0.01\theta_E$. Note that this is a worst-case scenario in several respects, with more concentrated or smaller galaxies being less affected. If the lens were Abell 1689, this would correspond to a $z = 1$ galaxy of FWHM $\sim 1''$ (Clowe & Schneider 2001), which is amongst the largest 1% of Leauthaud et al. (2007)'s catalog at magnitude $i' = 25$.

The main panel of figure 1b shows the measured ellipticity of the raytraced images, and the prediction of linear and higher order models. These converge away from the lens; the slight difference between them and the raytraced version is an effect of image pixellization. Pixellization errors are at the level of the separation between the curves, and are converging slowly. Near the lens, our non-linear model (19) again presents a worst case of the deviation from a linear prediction. It differs from the raytraced measurements due to even higher order terms in the coordinate transformation.

4. Discussion

We have derived the next-highest terms in the coordinate transformation relevant for weak gravitational lensing, by dropping the assumption of "local linearity". The resulting equations are hardly elegant, but can be simplified by making several reasonable assumptions about the galaxy's intrinsic shape and the lens profile. As expected, the perturbations from linear lensing theory are greatest for large galaxies; they increase as the size of the galaxy squared. As for gravitational flexion, this is simply due to the accumulating change in shear signal across the width of each image.

A linear lensing analysis systematically overestimates the shear signal near the core of galaxy clusters. However, even in the worst case scenario, it is acceptable surprisingly far into the non-linear regime. Assuming a value of 1.6 for the denominator of equation (12), it is within 1% of the true shear outside $\sim 1.07\theta_E$. We therefore conclude that this will be of only minor concern for measurements of the overall mass of individual (or even stacked) clusters in immediately forthcoming surveys. Most of the total signal comes from the large wings of a cluster, and the non-linear effects are currently outweighed by other potential sources of error. However, the effect ought to be considered by programs measuring the inner slopes of cluster mass distributions or the mass power spectrum on small scales. The effect can become relevant at about the level of statistical accuracy proposed for next-generation surveys.

We have not investigated the correction for a point spread function or the use of a weight function while measuring galaxy shapes. We have argued that this should perturb our results only slightly. However, a full analysis would be interesting in future work.

The authors thank Douglas Clowe, Yannick Mellier and Barnaby Rowe for useful discussions. This work was supported by NASA grant ATP04-0000-0067 and DoE grant FG02-04ER41316.

REFERENCES

Bacon D., Goldberg D., Rowe B. & Taylor A., 2006, MNRAS 365, 414

Bartelmann M. & Schneider P., 2000, Phys. Rep. 340, 291

Benjamin J. et al., 2007, MNRAS submitted (astro-ph/0703570)

Clowe D. & Schneider P., 2001, A&A 379, 384

Clowe D., Bradac M., Gonzalez A., Markevitch M., Randall S., Jones C. & Zaritsky D., 2006, ApJ 648, 109

Gavazzi R. & Soucail G., 2007, A&A 462, 459

Goldberg D. & Natarajan P., 2002, ApJ 564, 65

Goldberg D. & Bacon D., 2005, ApJ 619, 741

Heymans C. et al., 2006, MNRAS 371, 750

Kaiser N., Squires G. & Broadhurst T., 1995, ApJ 449, 460

Kitching T., Heavens A., Taylor A., Brown M., Meisenheimer K., Wolf C., Gray M. & Bacon D., 2007, MNRAS 374, 1377

Leauthaud A. et al., 2007, ApJS 172, 219

Massey R. et al., 2007, MNRAS 376, 13

Massey R. et al., 2007, Nature 445, 286

Massey R. et al., 2007, ApJS 172, 239

Mellier Y., 1999, ARA&A 37, 127

Miyazaki S. et al., 2007, ApJ in press (arXiv:0707.2249)

Refregier A., 2003, ARA&A 41, 645

Schirmer M., Erben T., Hetterscheidt M. & Schneider P., 2007, A&A 462, 875

Seitz S. & Schneider P., 1995

Smith R., Peacock J., Jenkins A., White S., Frenk C., Pearce F., Thomas P., Efstathiou G. & Couchmann H., 2003, MNRAS 341, 1311

Wittman D., 2005, ApJL 632, 5

This 2-column preprint was prepared with the AAS LaTeX macros v5.2.